Yang *et al. Biochar* (2024) 6:23
https://doi.org/10.1007/s42773-024-00311-8

Biochar

ORIGINAL RESEARCH Open Access

Valorising lignocellulosic biomass to high-performance electrocatalysts via anaerobic digestion pretreatment

Juntao Yang[1,2], Songbiao Tang[2], Wenjie Mei[2], Yiquan Chen[2], Weiming Yi[1], Pengmei Lv[2] and Gaixiu Yang[2*]

Abstract

Anaerobic digestion (AD) was initially evaluated as a potential preprocessing method for preparing biomass-based carbon electrocatalysts in this study. The AD pretreatment succeeded in the structural depolymerization and nitrogen enrichment of *Hybrid Pennisetum*, which provided favorable conditions to achieve efficient and homogeneous nitrogen introduction due to microorganism community enrichment and provided a porous structure by degradation of the biodegradable components. The resulted biochar exhibited improved physiochemical properties including higher specific surface areas, nitrogen content and graphitization degree than that obtained from pyrolyzing raw biomass. These improvements were positively correlated with the AD time and showed to have enhanced the performance in oxygen reduction reaction and practical microbial fuel cell applications. Amongst the investigated samples, the obtained biochar pretreated by AD for 15 days exhibited the most excellent performance with an onset potential of 0.17 V (VS. saturated calomel electrode) and the maximal power density of 543.2 mW cm^{-2} assembled in microbial fuel cells. This study suggested applying AD as a new biological pretreatment in the preparation of biomass-based electrocatalysts, and provided a unique pathway for fabricating high-performance biochar-based catalysts by structure optimization and N-containing active sites construction via gentle biological method, thereby providing a cost-effective method to fabricate metal-free catalysts for oxygen reduction reaction.

Highlights

- Anaerobic digestion pretreatment was conducted to assist electrocatalyst preparation.
- The biological pretreatment succeeded in carbohydrates decomposition and nitrogen enrichment.
- Pretreatment derived biochar significantly increased the ORR activity and microbial fuel cell performance.

Keywords Biomass, Anaerobic digestion, Biochar material, Oxygen reduction reaction, Electrocatalysis

Handling editor: Kitae Baek

*Correspondence:
Gaixiu Yang
yanggx@ms.giec.ac.cn
Full list of author information is available at the end of the article

Graphical Abstract

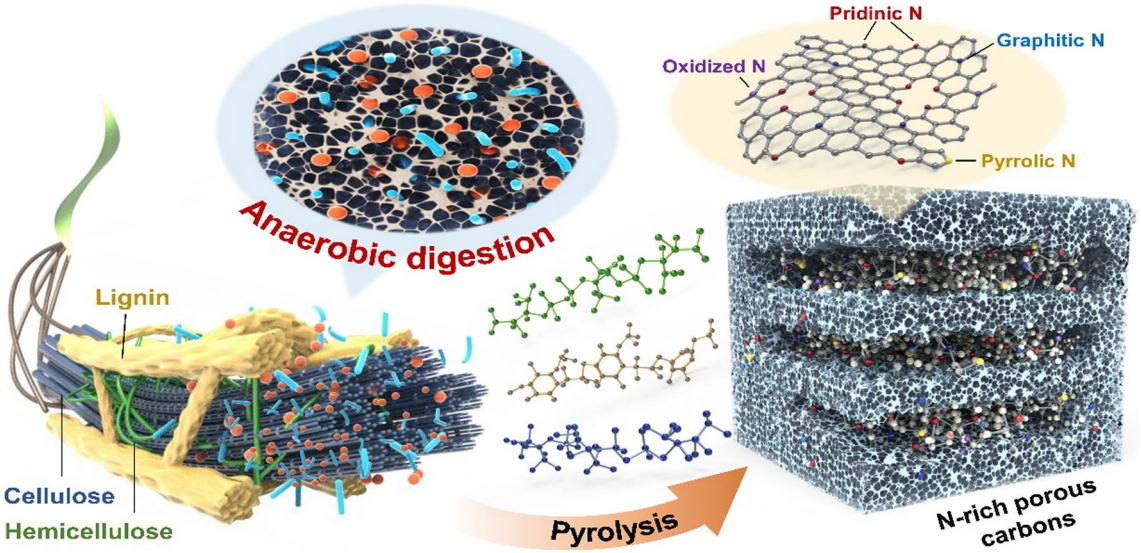

1 Introduction

The sustainable development of human beings is challenged by energy crisis and environmental pollution, and advanced technology is called for to realize circular bio-economy. to enable a circular bioeconomy. The application of microbial fuel cells (MFCs) is considered as an efficient and environmentally friendly approach that can achieve mild conversion of biodegradable organic wastes into green electricity. However, the practical implementation of MFC technologies is hindered by their sluggish oxygen reduction reaction (ORR) kinetics (Wan et al. 2020). Platinum (Pt)-based catalysts are extensively used as cathode materials for the ORR because they generate high catalytic activity, but they are also costly, scarce, and prone to poisoning (Li et al. 2022; Liu et al. 2022b). Therefore, it is imperative to develop electrocatalytic materials with high efficiency, low cost, high-activity ORR to replace this precious metal.

Biomass-derived carbon materials are promising substitutes for Pt-based catalysts because of their advantages such as low cost, stable structure, and excellent catalytic activity (Li et al. 2020). In previous studies, the preparation of biochar from various biomass resources, such as giant water hyacinth (Liang et al. 2018), Enteromorpha (Zhang et al. 2019), microalgae (Ma et al. 2020), pomelo peels (Maliutina et al. 2021), and cornstalks (Liu et al. 2022a), as well as their application for ORR were reported. However, pristine biochar materials generally exhibit poor catalytic activity (Ma et al. 2021). Pretreatment is therefore necessary to improve the ORR catalytic performance of biochar.

Pretreatment techniques can be categorized into physical, chemical, thermal and biological techniques (Fakayode et al. 2020; Yaashikaa et al. 2023). Physical pretreatment methods such as ball milling, densification, and extrusion can improve the physical properties of the biomass and its derived biochar (Meng & Wang 2020; Wannasen et al. 2022). However, the physical and chemical properties of biochar can be only improved to a limited extent. Thermal and chemical pretreatments effectively improve the properties of biomass derived biochar. However, their further development was restricted by the requirement of heat input and the use of hazardous chemicals, such as acids (Chu et al. 2018), alkalis, salts (Chen et al. 2021), and processes are energy intensive.

Recently, biological pretreatments have been used to assist the synthesis of high-efficiency ORR biochar catalysts. For instance, Wang et al. prepared porous carbon with ultrahigh specific surface area using the superior infiltrability and biodegradability of white-rot fungi on a lignocellulosic substrate (Wang et al. 2019). Peng et al. fabricated N-doped hierarchical porous carbon via enzymatic treatment and subsequent pyrolysis with ammonium chloride (NH_4Cl) (Peng et al. 2019). It was also suggested that the addition of NH_4Cl can impact the decarbonylating and decarboxylation reactions during the pyrolysis of oat straw, thereby promoting the degree of carbonization (Jerzak et al. 2023). The results of both

studies demonstrated that biological methods can effectively improve the physicochemical properties of biomass derived biochar.

Applying anaerobic digestion (AD) as a mild pretreatment also provides an opportunity to optimize the physiochemical properties of biochar. Compared with single-enzyme bacterial treatment, AD is also capable to partially decompose the biomass structure. In addition, microorganisms can be used as nitrogen sources possibly leading to the synthesis of N–doped carbon materials. Partial decomposition and nitrogen sources provide opportunities to produce porous N-doped biochar, which is promising for achieving the desired electrocatalytic performance. The AD process also produces biomethane as an added value, and the co-production of biogas and high-performance biochar will enable the complete valorisation of biomass resources. However, the application of AD to fabricate lignocellulosic biomass and enhance the properties of the resulting carbon materials has rarely been reported.

The aim of this study was to develop a proof-of-concept of using AD as a pretreatment for the preparation of N-doped carbon materials with *Hybrid Pennisetum* (HP) as the raw material. The effect of AD pretreatment on the physicochemical properties of the pretreated biomass and derived biochar materials was investigated. The obtained biochar was further used as a catalyst for the ORR and microbial fuel cells to investigate its electrocatalytic performance. Furthermore, the effects of AD pretreatment were compared with those of other previously used methods. The results of this study provide guidance for the development of mild and effective methods for valorising biomass to valuable products.

2 Experimental

2.1 Materials

HP was collected from Dingnan City, Jiangxi Province, China. Before using, the HP was washed with deionized water to remove surface impurities and then crushed. The inoculum obtained from the AD of the cow dung in a dairy farm in Guangzhou was domesticated in the laboratory for more than 2 weeks.

2.2 Pretreatment of catalyst precursors

AD was employed for HP pretreatment. Details are reported in our recent study (Yang et al. 2023a). Briefly, biomass pretreatment was performed in batch reactors (2 L). For each sample, 150 g of wet HP and 1600 mL of inoculum were mixed and kept at a mesophilic temperature (37 ± 1 °C) for up to 15 days. The solid digestate was collected after the hydraulic retention times of 3, 9, and 15 days. Solid products were dried and crushed into biochar catalyst precursors. The obtained biomass precursors were named as PH-X (where PH represents the raw material and X represents the days of digestion).

2.3 Preparation of biochar catalysts

Biochar catalysts were prepared via the pyrolysis of various pretreated HP. Pyrolysis experiments were carried out at 800 °C in a programmed temperature-controlled tube furnace. In each run, 2 g raw material was placed in the middle of a quartz tube, heated to 800 °C at 5 °C min^{-1} under a N_2 atmosphere with a flow rate of 200 mL min^{-1} and retained for 2 h. The solid product was collected when it reached room temperature. The collected product was washed with 1 M HCl solution for 24 h, filtered with deionized water until it reached a neutral pH, and then dried overnight at 60 °C. The obtained catalysts were named as C-PH-X (where PH represents the raw material and X represents the days of digestion).

2.4 Characterization

The elemental analysis of raw materials was carried out by using an elemental analyzer (ario EL, Elementar, Germany). The contents of cellulose, hemicellulose and lignin were measured according to the National Renewable Energy Laboratory (NREL) standard (Wu et al. 2021). The morphologies and the texture properties of the prepared materials were estimated using the scanning electron microscope (SEM, JEOL JSM-7600F). A nitrogen adsorption–desorption test was performed using a gas adsorption analyzer (ASIQMO002-2). The specific surface area of catalyst was evaluated by the Brunauer – Emmett – Teller (BET) method, and the pore size distribution of catalyst was calculated based on the density functional theory (DFT) method. The crystalline phase of the obtained catalyst was analyzed by X-ray diffraction (XRD, Model D/max-rC) using a Cu Kα radiation source with λ of 1.5406 Å. The content and species of nitrogen on the catalyst surface were determined by X-ray photoelectron spectra (XPS, Thermo Fisher ESCALAB250Xi spectrometer). The types of functional groups on the surface of the gained catalyst were analyzed by Fourier transform infrared spectrometer (FTIR, Bruker, TENSOR27).

2.5 Electrochemical tests

The electrochemical measurements were carried out in a conventional three-electrode cell connected to the CHI 760E electrochemical workstation (Chenhua Co., Ltd. Shanghai, China). A glassy carbon electrode, a Pt wire and a saturated calomel electrode (SCE) were used as the working electrode, counter electrode and reference electrode, respectively. The cyclic voltammetry (CV) and linear-sweep voltammetry (LSV) curves were measured by the rotating disk electrode (RDE) in N_2 or O_2 saturated

50 mM phosphate buffer solution (PBS) at 10 mVs $^{-1}$. The Tafel slopes were calculated according to our previous work (Yang et al. 2023a), where i_k is the kinetic current density.

Rotating ring disk electrode (RRDE) tests were performed to evaluate the number of electron transfer (n) and hydrogen peroxide (H_2O_2) yield. These tests were performed under N_2 or O_2 in saturated 50 mM PBS at 10 mVs $^{-1}$ with 1600 rpm. The electron selectivity of the catalysts was evaluated based on the electron transfer number (n) and H_2O_2 yield, which were determined by the following equations (Gong et al. 2020):

$$n = 4\frac{I_d}{I_d + I_r/N} \quad (1)$$

$$H2O2\% = 200\frac{I_r/N}{I_d + I_r/N} \quad (2)$$

where I_d is the disk current, I_r is the ring current, and N = 0.37 is the current collection efficiency of Pt ring.

The assembly of the MFCs was carried out according to the method introduced in a previous study (Yang et al. 2023b). The detailed description is presented in the supplementary information (SI). The voltage output was recorded by a data collector (Tektronix, Keithely 2700E) and the polarization curves of MFCs were measured according to the steady discharging method.

3 Results and discussion

3.1 Physiochemical properties of biomass and AD-pretreated biomass

The SEM images of the raw HP and AD-pretreated samples are shown in Fig. 1. The biomass morphologies of biomass were significantly different with the increasing AD time. Undigested HP (Fig. 1a) displayed a highly compact and intact surface texture, whereas HP treated with AD showed a porous and rough surface (Fig. 1b–d), as well as many shallow nanoholes. After AD treatment for 15 d (Fig. 1d), the surface structure of HP-15 was severely etched and abundant channels with varying erosion holes appeared. These results can be mainly attributed to the digestion of biomass components (cellulose and hemicellulose) with the increase of AD time. Specific compositional changes are shown in Additional file 1: Fig. S1. After AD pretreatment for 15 d, the relative contents of cellulose and hemicellulose decreased from 34.73% to 10.99% and 20.53% to 8.42%, respectively, and 75 wt.%

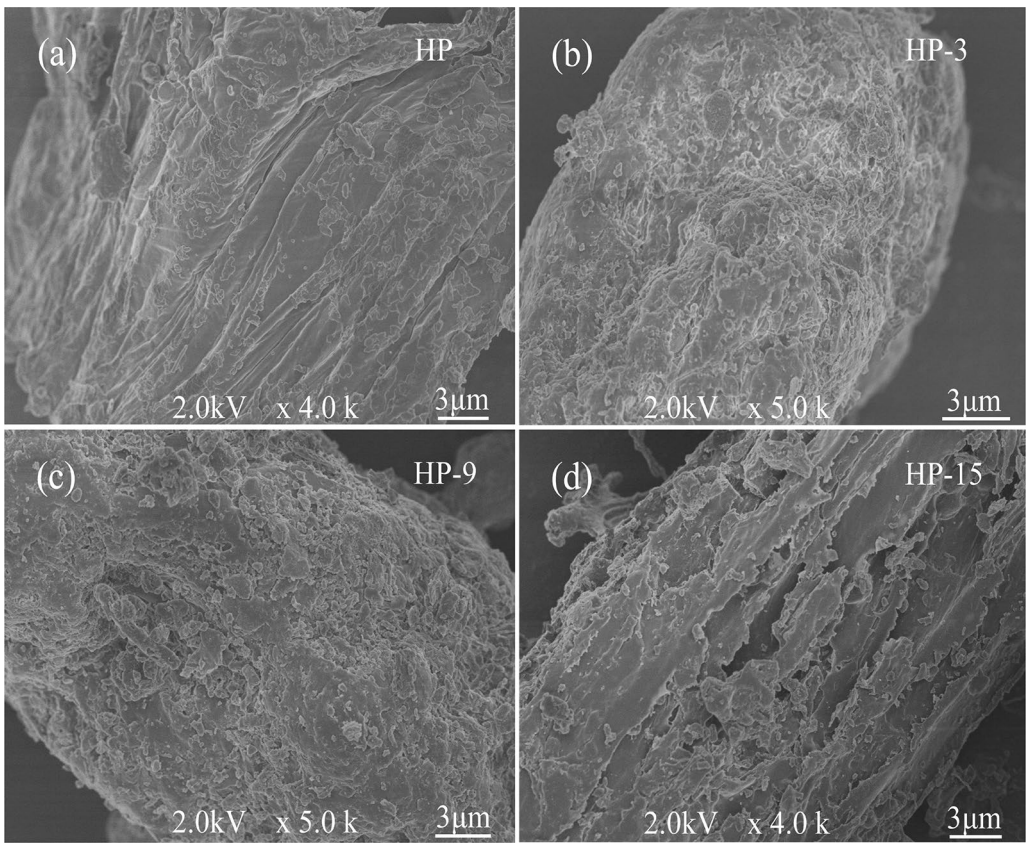

Fig. 1 SEM images of HP (**a**), HP-3 (**b**), HP-9 (**c**), and HP-15 (**d**)

of the raw biomass was degraded. It can be assumed that this drastic decrease effectively altered the biomass structure, as presented in Fig. 1. Thus, loose and porous structured biomass can be used as an ideal feedstock to produce porous biochar. The ultimate analysis results for all biomass precursors are presented in Additional file 1: Table S1. With an increase in the AD time, the relative contents of C and O decreased, whereas the N concentration increased, indicating that mainly carbohydrates (hemicellulose and part of cellulose) in the biomass were consumed during AD, and microbial cells (rich in N) constantly accumulated in the solid digestate (Wang et al. 2023). The accumulation of N provides favorable conditions for the synthesis of N-doped biochar.

3.2 Physiochemical properties of biochar materials

The obtained AD-pretreated biomass was pyrolyzed under the same conditions (800 °C for 2 h) to produce biochar. The SEM images of various samples are shown in Additional file 1: Fig. S2. C-HP displayed a smooth surface, which became rougher with visible pores and channels after AD pretreatment. This observation was consistent with the SEM characterization of pretreated biomass. To further analyze the changes in structural features, the pore structures of the samples were measured using N_2 adsorption-desorption isotherms. As shown in Fig. 2a, all samples exhibited typical hysteresis loops, which strongly implied the existence of mesopores (Qunying et al. 2014). Compared with the other samples, C-HP-15 showed a drastic increase in N_2 adsorption at a relatively low pressure ($P/P_0 < 0.01$), indicating that it contained more well-developed micropores. The specific surface areas and pore volumes of all samples are summarized in Table 1. The specific surface area of obtained biochar materials increased with the extension of AD time in the order of C-HP-15 (225 m^2g^{-1}) > C-HP-9 (209 m^2g^{-1}) > C-HP-3 (175 m^2g^{-1}) > C-HP (120 m^2g^{-1}). The pore size distribution also confirmed the microporous structure of C-HP-15 (Fig. 2b). In contrast to other biochar materials with a main pore size ranging from 2.4 to 10.0 nm, C-HP-15 pore size fell in the range of micropores (1.3–2.0 nm).

The crystallinities of the biochar catalysts were determined using XRD. As shown in Fig. 3a, all the samples exhibited peaks at 25° and 43.5°, corresponding to the (002) and the (100) crystal plane of carbon, respectively. The (002) and (100) diffraction peaks indicated a layer-to-layer d-spacing of 0.34 and 0.243 nm, respectively, which can be attributed to the diffraction of the graphitic structure. The broad diffraction halo peak at 25° and relatively weak diffraction peak at 43.5° indicate that carbon is disordered. FT-IR spectroscopy was employed to investigate changes of surface functional groups of the biochar catalysts. Figure 3b reveals that all

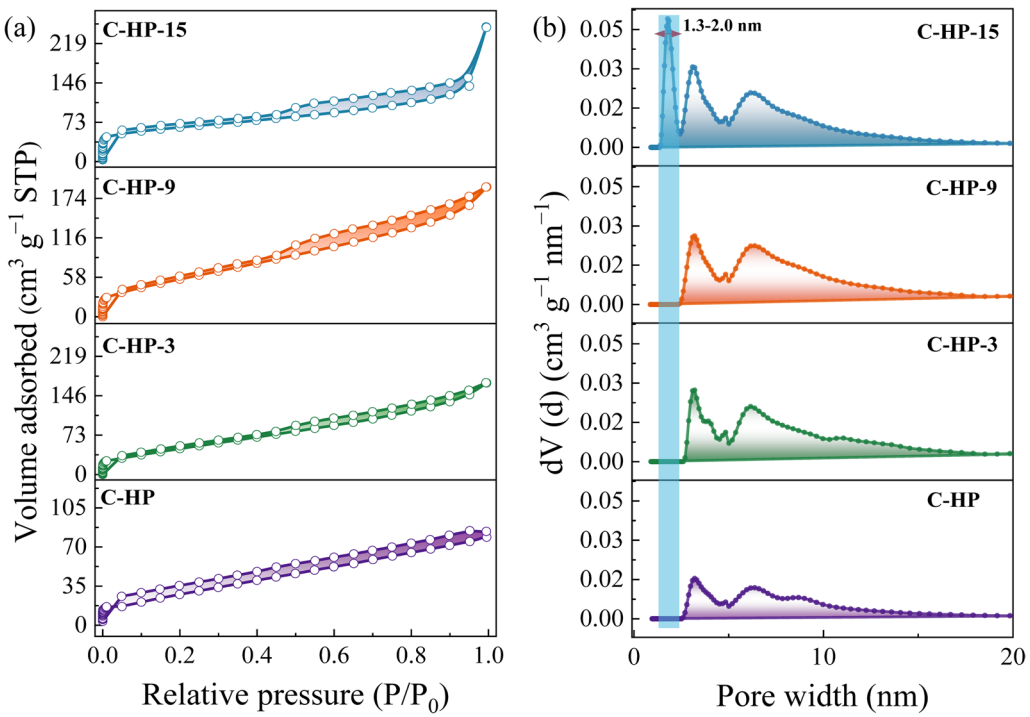

Fig. 2 N_2 adsorption–desorption isotherms (**a**) and pore size distribution (**b**) of C-HP, C-HP-3, C-HP-9, and C-HP-15

Table 1 Summary of textural parameters obtained from nitrogen adsorption analysis of C-HP, C-HP-3, C-HP-9, and C-HP-15

Sample	S_{BET} (m^2g^{-1})	S_{micro} (m^2g^{-1})	S_{meso} (m^2g^{-1})	V_{total} (m^2g^{-1})	V_{micro} (m^2g^{-1})	V_{meso} (m^2g^{-1})
C-HP	120	0	120	0.13	0	0.13
C-HP-3	175	0	175	0.26	0	0.26
C-HP-9	209	0	209	0.30	0	0.30
C-HP-15	225	78	147	0.39	0.04	0.35

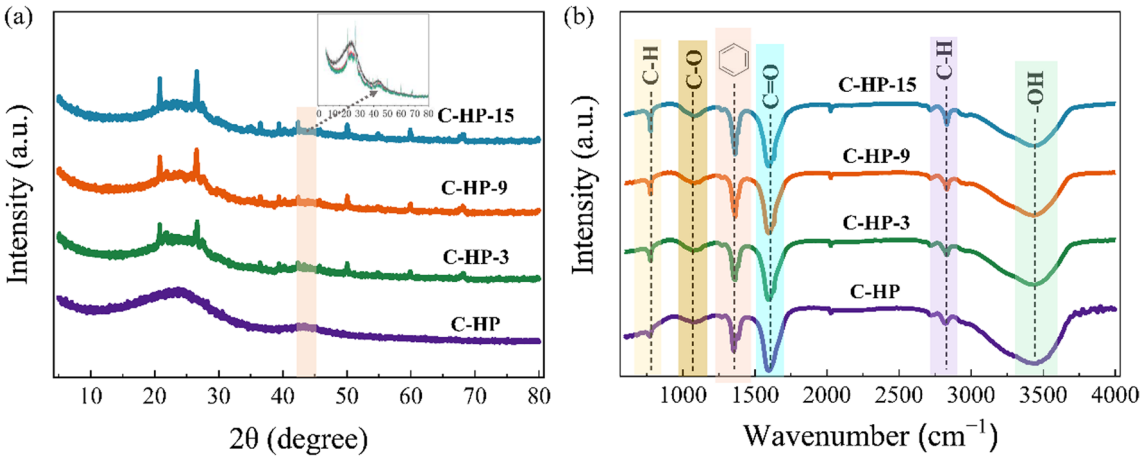

Fig. 3 XRD (a) patterns and FT-IR spectra (b) of C-HP, C-HP-3, C-HP-9, and C-HP-15

biochar catalysts had similar peaks at 763, 1056, 1361, 1608, 2829, and 3448 cm^{-1}, corresponding to the tensile vibrations of C(aryl)–CH_X, C–O, -aryl, C=O, –CH_X and –OH, respectively (Najbjerg et al. 2011; Sun et al. 2018). The peak intensities of C(aryl)–CH_X and -aryl increased in the order of C-HP-15 > C-HP-9 > C-HP-3 > C-HP, indicating that an increase in the AD time improves the graphitization of the obtained biochar catalyst. In addition, the peak intensities of several oxygenated functional groups, such as C=O and –OH, decreased in the order C-HP-15 < C-HP-9 < C-HP-3 < C-HP. This may be attributed to the increase in the degree of degradation of the hydroxy-rich cellulose and hemicellulose in the biochar precursor with increasing AD time, because many oxygen bearing substances mainly originate from cellulose and hemicellulose in the pyrolysis process (Xiong et al. 2023). Raman spectroscopy was conducted to determine the degree of graphitization and defects in the biochar catalysts. As depicted in Additional file 1: Fig. S3, two peaks can be observed at 1350 and 1590 cm^{-1}, which can be attributed to the D (disordered carbon) and G (graphitic carbon) bands of the biochar catalyst. The G-band originates from in-plane stretching vibrations of all sp^2 hybrid atoms in the graphitic structure. The D-band is related to defects and disordered structures caused by vacancies and heteroatom doping. The I_D/I_G ratio is generally used to characterize the defects and graphitic degree of carbon materials. An increase of the I_D/I_G ratio indicates an increase in the defect degree (Wu et al. 2018). The I_D/I_G ratio of the biochar catalysts varied from 1.06 to 1.11, and no significant changes were observed.

XPS characterization was conducted to investigate the types of N-doping on the carbon structure. As shown in Fig. 4, the N 1s spectra of all catalysts can be resolved into four peaks at 398.4, 398.4, 401.4, and 402.0 eV, which correspond to pyridinic-N, pyrrolic-N, graphitic-N, and oxidic-N, respectively (Hu et al. 2020; Ma et al. 2020). Compared with C-HP, the intensities of the N 1s peaks of C-HP-3, C-HP-9 and C-HP-15 were enhanced, indicating that the biochar catalysts (C-HP-3, C-HP-9 and C-HP-15) obtained after AD treatment contained more N in the carbon skeleton than the untreated biochar catalyst (C-HP). Furthermore, N enrichment in the precursor after AD treatment could effectively increase the N-doping amount of the biochar. It is worth noting that the relative contents of pyridinic-N and graphitic-N in the biochar catalysts increased in the order C-HP-15 > C-HP-9 > C-HP-3 > C-HP (Table 2). Pyridinic-N and graphitic-N have been reported to be responsible to the ORR activity of biochar catalysts (Guo et al. 2016). This

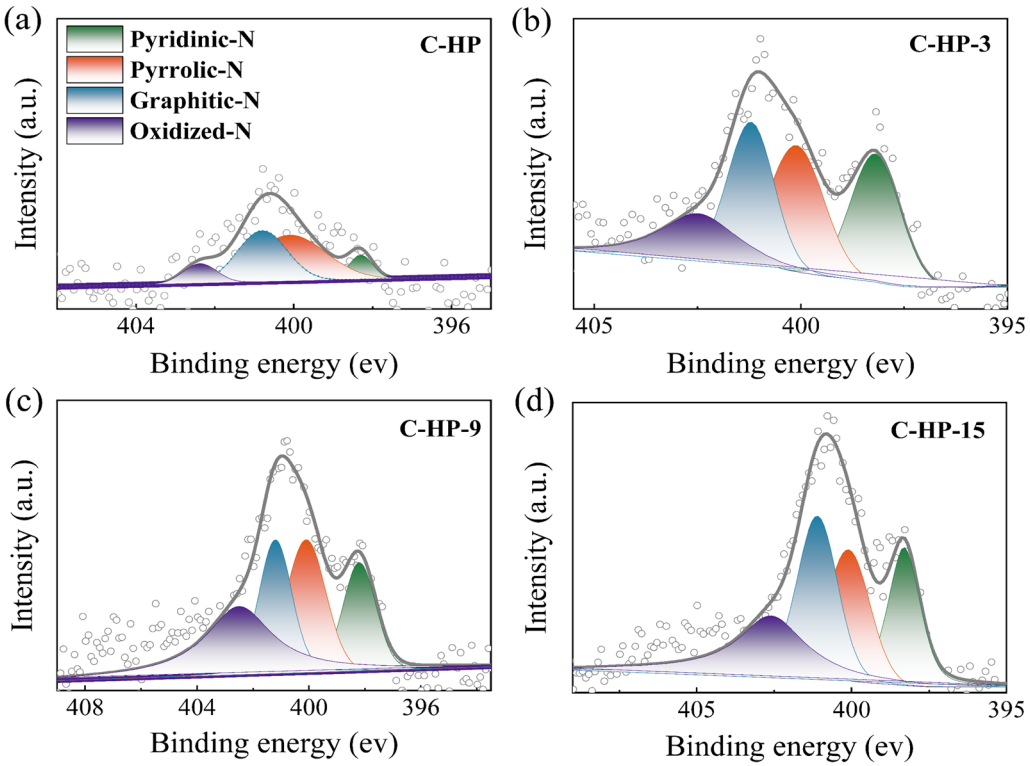

Fig. 4 N1s spectrum of C-HP (**a**), C-HP-3 (**b**), C-HP-9 (**c**), and C-HP-15 (**d**)

Table 2 The relative content of the sum of pyridinic-N, pyrrolic-N, graphitic-N and oxidized-N for C-HP, C-HP-3, C-HP-9 and C-HP-15

Name	Pyridinic-N (%)	Pyrrolic-N (%)	Graphitic-N (%)	Oxidized-N (%)
C-HP	11.0	64.3	19.5	5.2
C-HP-3	17.8	39.7	23.7	18.8
C-HP-9	18.1	29.5	28.9	23.5
C-HP-15	22.6	24.3	29.0	24.1

is because (1) pyridinic-N produces active sites during the chemisorption of oxygen; thus, the reduction of O_2 is more efficient (Wang et al. 2018), and (2) graphitic-N might be responsible for the reduction of oxygen through a four-electron pathway (Duan & Henkelman 2020; Liu et al. 2016).

3.3 The ORR electrochemical performance and practical MFC application performance

To examine the electrocatalytic activity of the biochar catalysts, CV was conducted in 50 mM PBS with oxygen or nitrogen. As shown in Additional file 1: Fig. S4, all the biochar catalysts showed distinct peaks in the O_2-saturated solution, whereas ORR peaks were not observed for any sample in the N_2-saturated solution. These results revealed that all biochar catalysts exhibited ORR catalytic activity. Furthermore, LSV measurements were performed in an O_2-saturated 50 mM PBS environment at 1600 rpm. Generally, a positive onset potential (E_{onset}) of an electrocatalyst indicates its high electrocatalytic ORR performance. Figure 5a shows that the E_{onset} of the catalysts ranked as follows: C-HP (-0.07 V vs. SCE) < C-HP-3 (0.12 V vs. SCE) < C-HP-9 (0.15 V vs. SCE) < C-HP-15 (0.17 V vs. SCE). This indicates that the ORR activity of the obtained biochar catalyst increased and oxygen more easily electrochemically reduced with increasing AD time (Yang et al. 2018). To gain insights into the kinetics parameters of ORR catalysis, the Tafel slope was calculated. A low Tafel slope implied enhanced kinetics (Jose et al. 2021). As shown in Fig. 5b, the Tafel slopes of the biochar catalysts decreased in the order of C-HP-15 < C-HP-9 < C-HP-3 < C-HP, which further confirms that the ORR activity and kinetics increased with the increase of AD time. This improvement is likely due

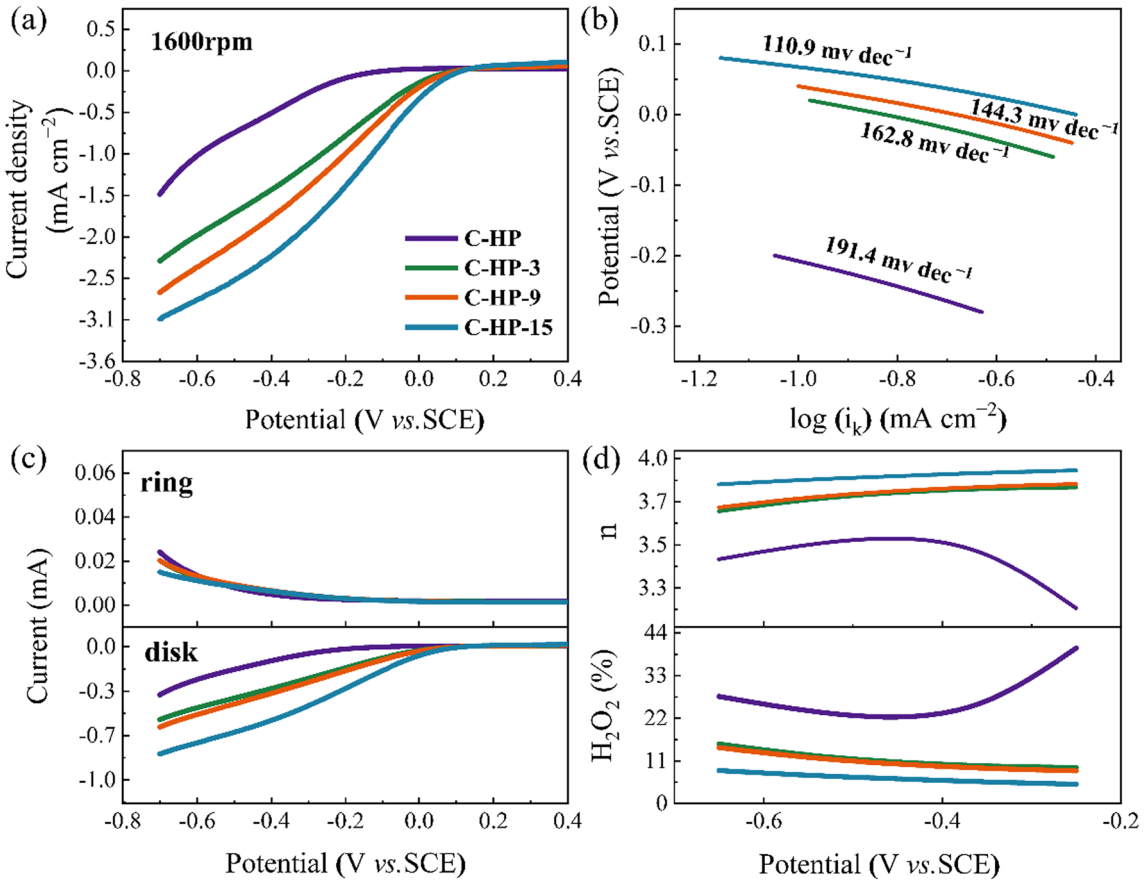

Fig. 5 LSV curves of samples in O_2-saturated 50 mM PBS at 1600 rpm (**a**) and corresponding Tafel slope (**b**); RRDE tests of the ORR on samples in O_2-saturated 50 mM PBS electrolyte at a rotation rate of 1600 rpm (**c**); Hydrogen peroxide yields (H_2O_2%) and the electron number (n) calculated from RRDE on C-HP, C-HP-3, C-HP-9 and C-HP-15 (**d**)

to the increase of the graphitic-N and pyridinic-N (Li et al. 2016).

Generally, the ORR is a multi-step process, which mainly occurs through 2e- and 4e- pathways (Zhang and Xia 2011). As shown in the equations of (3, 4), it is worth noting that the 4e$^-$ pathway is the desired one for the ORR process as the 2e- pathway generates H_2O_2, which can lead to the increase of over potential (Li et al. 2021).

$$O2 + 4H^+ + 4e^- = 2H2O \quad (3)$$

$$O2 + 2H^+ + 2e^- = H2O2 \quad (4)$$

The electron transfer number is an important index for evaluating the reaction kinetics of ORR electrocatalytic materials (Zhou et al. 2023). The disk ring currents of the biochar catalysts were determined using RRDE measurement (Fig. 5c), and the electron transfer numbers (n) were calculated using Eq. (1). When the AD time increased to 15 d, the electron transfer number of the obtained biochar catalyst reached nearly 4, indicating that the ORR of using C-HP-15 is mainly through the 4e- transfer pathway. Furthermore, to verify the electron transfer pathway of the catalysts, the H_2O_2 yield was analyzed. As the reaction approaches four-electron transfer, the yield of H_2O_2 decreases. Figure 5d shows that the yield of H_2O_2 decreased in the order of C-HP-15 < C-HP-9 < C-HP-3 < C-HP, suggesting that the four-electron ORR strengthened with increasing AD time.

MFCs were assembled with various biochar as cathode catalysts to investigate their practical application performance (Additional file 1: Fig. S5). The MFCs using biochar as air–cathode materials remained stable within 6 operating cycles (Fig. 6a). During each of the running cycle, the output voltage of MFCs with different cathode catalysts increased in the order of C-HP-15 > C-HP-9 > C-HP-3 > C-HP, and the maximal output voltage of MFCs reached 303 mV with C-HP-15 as the cathode, which is 1.4 times higher than that of the C-HP (221 mV). This indicates that the AD pretreatment derived biochar as cathode catalyst enhanced ORR performance and improved the power generation

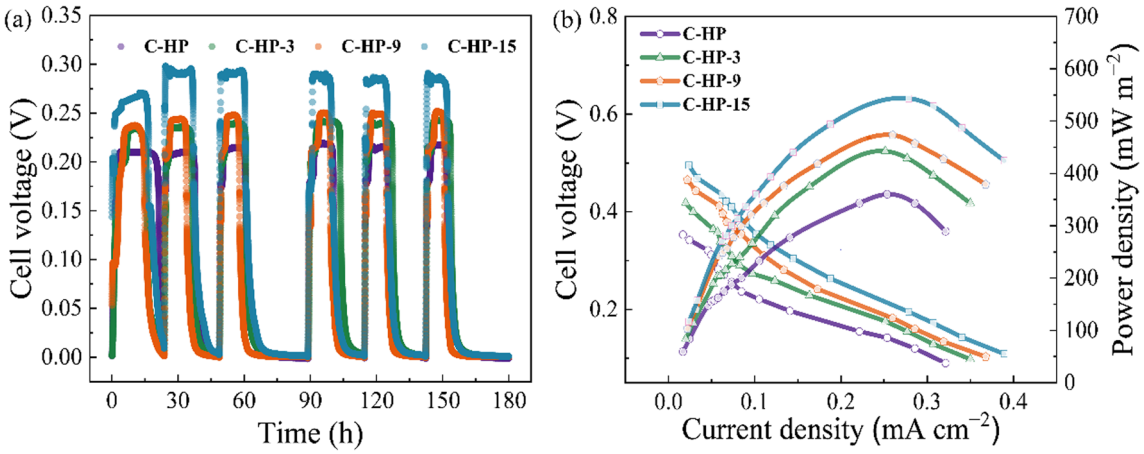

Fig. 6 The run cycles (**a**), Power-density curves and cell-polarization curves (**b**) of MFCs with C-HP, C-HP-3, C-HP-9 and C-HP-15

performance of MFCs. According to the power density curves in Fig. 6b, the peak power densities of the MFCs with different catalysts were 543.2, 473.2, 442.5, and 360.1 mW cm^{-2} for C-HP-15, C-HP-9, C-HP-3, and C-HP, respectively. Considering that the experiments were performed under the same conditions except for the cathode catalyst, the output voltage and power density should be attributed to cathodic biochar and C-HP-15 was shown to have the most significant performance. This further confirms that increasing the AD pretreatment time enhanced the power generation performance of MFCs, which is consistent with the output voltage analysis.

3.4 Further discussions

Electrochemical catalytic performances of carbon materials strongly depend on their physicochemical properties. Achieving excellent ORR activity in carbon catalysts requires multi-dimensional engineering including appropriate heteroatom doping, porous structure adjustment, and high graphitization (Xu et al. 2021). Specifically, increasing the abundance of mesopores could benefit mass transport during the reaction (Xu et al. 2021). A higher specific surface area provides more opportunities to obtain more active sites (Kaur et al. 2019). Higher graphitization indicates a better electrical conductivity of biochar. N-doping with higher graphitic-N and pyridinic-N concentrations can yield numerous active sites (Li et al. 2016).

In this study, AD successfully achieved the partial degradation of lignocellulosic biomass composites, and 75% of the hemicellulose and cellulose were digested, resulting in a lignin-rich residue. In addition, the surface structure was altered with an abundant porous structure, which enhanced the specific surface area of the obtained biochar. Similar results were also achieved by physical and chemical methods (Gao et al. 2020). Interestingly, both the pretreated biomass and resulting biochar had higher nitrogen contents, which eventually led to higher abundance of graphitic-N and pyridinic-N, both of which have been previously reported as keys to enhance the ORR performance of biochar (Duan & Henkelman 2020). The improved MFC application performance of AD-pretreated biochar further confirmed that this mild pretreatment is viable for enhancing the electrocatalytic properties of biochar. The analysis results showed that the biochar obtained with AD pretreatment had a richer mesopore structure, larger specific surface area, higher graphitization, and higher contents of graphitic-N and pyridinic-N than untreated biochar. Each of these improvements is beneficial for achieving a better catalytic performance.

Recent representative studies using different pretreatment methods for biochar preparation and ORR are listed in Table 3. Compared with other biochar electrocatalysts, the samples prepared in this study did not show a superior reversible E_{onset}. This might be owing to various factors such as the application of different activation methods, inconsistency of raw materials, and different pyrolysis conditions. However, it should be noted that the AD pretreatment conducted in this study achieved a maximal increase in E_{onset} by 0.24 V in 50 mM PBS. This enhancement was significantly higher than that reported in other studies. Furthermore, the increase in E_{onset} under alkaline conditions was measured. Additional file 1: Fig. S6 and Table 3 show that the maximal increase of E_{onset} in 0.1 M KOH solution was 0.15 V, representing an excellent improvement. The AD pretreatment is a promising strategy for improving the electrocatalytic properties of lignocellulosic biomass. Based on the results of this study, more research should be conducted to optimize

Table 3 The comparison of the ORR performance between this work and other reported based on recent literature

Original biomass	Pretreatment method	Pyrolysis condition	ORR activity (E_{onset})		Increase of E_{onset}	Refs.
			Untreated	Pretreated		
Yuba	Ball-milling	850 °C for 2 h	0.97 V vs. RHE in 0.1 M KOH solution	0.97 V vs. RHE in 0.1 M KOH solution	0 V	(Zhang et al. 2021)
Pyrrolet	Freeze-drying	1000 °C for 2 h	0.92 V vs. RHE in 0.1 M KOH solution	0.97 V vs. RHE in 0.1 M KOH solution	0.05 V	(Kurian et al. 2022)
Brown coal	Oxidative (O_2) treatment	1050 °C for 2 h	0.905 V vs. RHE in 0.1 M KOH solution	0.978 V vs. RHE in 0.1 M KOH solution	0.073 V	(Liu et al. 2019)
Bamboo	Alkali (NaOH) treatment	900 °C for 1 h	~0.97 V vs. RHE in 0.1 M KOH solution	0.98 V vs. RHE in 0.1 M KOH solution	0.1 V	(Cui et al. 2023)
Cattail leaves	Alkali (ammonia) treatment	700 °C for 2 h	0.72 V vs. RHE in 0.1 M KOH solution	0.88 V vs. RHE in 0.1 M KOH solution	0.16 V	(Panomsuwan et al. 2022)
Hot-pressed rapeseed press cake	Acid (mixture of HNO_3 and H_2SO_4) treatment	800 °C for 2 h	0.90 V vs. RHE in 0.1 M KOH solution	0.92 V vs. RHE in 0.1 M KOH solution	0.02 V	(Juvanen et al. 2022)
Microalgae	Lipid extraction	800 °C for 2 h	0.75 V vs. RHE in 50 mM PBS	0.82 V vs. RHE in 50 mM PBS	0.07 V	(Wang et al. 2022)
Raw wood	Enzyme treatment	900 °C for 2 h	-	0.988 V vs. RHE in 0.1 M KOH solution	-	(Peng et al. 2019)
Hybrid Pennisetum	Anaerobic digestion	800 °C for 2 h	0.73 V vs. RHE in 0.1 M KOH solution	0.88 V vs. RHE in 0.1 M KOH solution	0.15 V	This work
Hybrid Pennisetum	Anaerobic digestion	800 °C for 2 h	0.58 V vs. RHE in 50 mM PBS	0.82 V vs. RHE in 50 mM PBS	0.24 V	This work

All potential units were converted to reversible hydrogen electrode (RHE) based on the previously introduced method (Wang et al. 2020; Ye et al. 2021)

the pretreatment and pyrolysis conditions for different types of biomass.

Furthermore, the proposed AD approach is capable of producing a fraction of biomethane, achieving added value from lignocellulosic biomass. Considering that this process is a mild treatment and that no hazardous chemicals are used, it is preferable over conventional chemical pretreatment. The economic viability needs to be further assessed as an energy-consuming drying process if required after AD. Based on the proof-of-concept developed in this study, the physicochemical parameters of biochar can be improved. For instance, augmentation with the desired AD microorganisms will further enhance the pretreatment performance. The nitrogen content can be further increased via co-AD with nitrogen-rich feedstocks such as food wastes. These research avenues should be further explored.

4 Conclusion

In this study, proof-of-concept research was conducted on the application of AD as a pretreatment for electrocatalytic biochar preparation. Upon digesting the majority of the biodegradable carbohydrates (hemicellulose and cellulose) in lignocellulosic biomass via AD, the porous structure of the biomass improved and the nitrogen content increased. Pyrolysis of pretreated biomass resulted in biochar material with an improved porous structure, higher specific surface area, enhanced graphitization and doping with abundant graphitic-N and pyridinic-N. This multi-dimensional improvement can enhance the ORR and MFC performances when biochar is used as an electrocatalyst. The results of this study lay the foundation for integrating AD and pyrolysis to achieve near-complete valorization of grass biomass to valuable products.

Supplementary Information

The online version contains supplementary material available at https://doi.org/10.1007/s42773-024-00311-8.

Additional file 1: Figure S1. The cellulose, hemicellulose and lignin content of HP, HP-3, HP-9 and HP-15. **Figure S2.** Structural characteristics of carbon catalysts. SEM images of (**a**) C-HP catalyst; (**b**) C-HP-3 catalyst; (**c**) C-HP-9 catalyst; (**d**) C-HP-15 catalyst. Figure S3. Raman spectrum of all obtained samples. Figure S4 CV curves of samples in O_2-saturated (solid line) or N_2-saturated 50 mM PBS solution (dash line). **Figure S5.** Physical map (**a**) and schematic illustration (**b**) of MFC. Figure S6 LSV curves of all samples in O_2-saturated 0.1 M KOH solution at 1600 rpm. **Table S1.** ultimate analyses of samples at different fermentation time.

Acknowledgements

The authors would like to thank the support of School of Agricultural Engineering and Food Science, Shandong University of Technology and Guangzhou Institute of Energy Conversion, Chinese Academy of Sciences (CAS Key Laboratory of Renewable Energy).

Author contributions

All authors contributed to the study conception and design. JY: Data curation, Writing. ST: Investigation, Data curation, WM and YC: Visualization. WY: Conceptualization, Supervision. PL: Conceptualization, Formal analysis. GY:

Conceptualization, Methodology, Writing- Reviewing and Editing. All authors read and approved the final manuscript.

Funding
This work was funded by the National Natural Science Foundation of China (52176214 and 52130610), the National Key R&D Program of China (2022YFC3902400), Shenzhen Science and Technology Program (JCYJ20200109150210400) and the Youth Innovation Promotion Association CAS (2020345).

Data availability
The datasets used or analyzed during the current study are available from the corresponding author on reasonable request.

Declarations

Competing interests
The authors have no competing interests to declare that are relevant to the content of this article.

Author details
[1]School of Agricultural Engineering and Food Science, Shandong University of Technology, Zibo 255049, Shandong, China. [2]Guangzhou Institute of Energy Conversion, Chinese Academy of Sciences (CAS Key Laboratory of Renewable Energy), Guangzhou 510640, China.

Received: 26 August 2023 Revised: 20 February 2024 Accepted: 21 February 2024
Published online: 12 March 2024

References

Chen J, Liu J, Wu D, Bai X, Lin Y, Wu T, Zhang C, Chen D, Li H (2021) Improving the supercapacitor performance of activated carbon materials derived from pretreated rice husk. J Storage Mater 44:103432. https://doi.org/10.1016/j.est.2021.103432

Chu G, Zhao J, Huang Y, Zhou D, Liu Y, Wu M, Peng H, Zhao Q, Pan B, Steinberg CEW (2018) Phosphoric acid pretreatment enhances the specific surface areas of biochars by generation of micropores. Environ Pollut 240:1–9. https://doi.org/10.1016/j.envpol.2018.04.003

Cui P, Li T, Chi X, Yang W, Chen Z, Han W, Xia R, Shimelis A, Iwuoha EI, Peng X (2023) Bamboo derived N-doped carbon as a bifunctional electrode for high-performance zinc–air batteries. Sustainable Energy Fuels 7:2717–2726. https://doi.org/10.1039/D3SE00315A

Duan Z, Henkelman G (2020) Identification of active sites of pure and nitrogen-doped carbon materials for oxygen reduction reaction using constant-potential calculations. J Phys Chem C 124:12016–12023. https://doi.org/10.1021/acs.jpcc.0c03951

Fakayode OA, Aboagarib EAA, Zhou C, Ma H (2020) Co-pyrolysis of lignocellulosic and macroalgae biomasses for the production of biochar—a review. Bioresour Technol 297:122408. https://doi.org/10.1016/j.biortech.2019.122408

Gao Y, Yue Q, Gao B, Li A (2020) Insight into activated carbon from different kinds of chemical activating agents: a review. Sci Total Environ 746:141094. https://doi.org/10.1016/j.scitotenv.2020.141094

Gong XB, Peng L, Wang XH, Wu LL, Liu Y (2020) Duckweed derived nitrogen self-doped porous carbon materials as cost-effective electrocatalysts for oxygen reduction reaction in microbial fuel cells. Int J Hydrogen Energy 45:15336–15345. https://doi.org/10.1016/j.ijhydene.2020.03.177

Guo D, Shibuya R, Akiba C, Saji S, Kondo T, Nakamura J (2016) Active sites of nitrogen-doped carbon materials for oxygen reduction reaction clarified using model catalysts. Science 351:361–365. https://doi.org/10.1126/science.aad0832

Hu X, Min Y, Ma L-L, Lu J-Y, Li H-C, Liu W-J, Chen J-J, Yu H-Q (2020) Iron-nitrogen doped carbon with exclusive presence of FexN active sites as an efficient ORR electrocatalyst for Zn-air battery. Appl Catal B-Environ 268:118405. https://doi.org/10.1016/j.apcatb.2019.118405

Jerzak W, Gajek M, Magdziarz A (2023) Oat straw pyrolysis with ammonium chloride doping: analysis of evolved gases, kinetic triplet, and thermodynamic parameters. Bioresour Technol 388:129784. https://doi.org/10.1016/j.biortech.2023.129784

Jose V, Nsanzimana JMV, Hu H, Choi J, Wang X, Lee J-M (2021) Highly efficient oxygen reduction reaction activity of N-doped carbon–cobalt boride heterointerfaces. Adv Energy Mater 11:2100157. https://doi.org/10.1002/aenm.202100157

Juvanen S, Sarapuu A, Mooste M, Käärik M, Mäeorg U, Kikas A, Kisand V, Kozlova J, Treshchalov A, Aruväli J, Leis J, Tamm A, Tammeveski K (2022) Electroreduction of oxygen on iron- and cobalt-containing nitrogen-doped carbon catalysts prepared from the rapeseed press cake. J Electroanal Chem 920:116599. https://doi.org/10.1016/j.jelechem.2022.116599

Kaur P, Verma G, Sekhon SS (2019) Biomass derived hierarchical porous carbon materials as oxygen reduction reaction electrocatalysts in fuel cells. Prog Mater Sci 102:1–71. https://doi.org/10.1016/j.pmatsci.2018.12.002

Kurian M, Ghosh M, Vijayakumar V, Pandinhare Puthiyaveetil P, Torris A, Kurungot S (2022) Influence of ice templating on oxygen reduction catalytic activity of metal-free heteroatom-doped mesoporous carbon derived from polypyrrole for zinc-air batteries. Energy Technol 10:2200840. https://doi.org/10.1002/ente.202200840

Li J-C, Hou P-X, Zhao S-Y, Liu C, Tang D-M, Cheng M, Zhang F, Cheng H-M (2016) A 3D bi-functional porous N-doped carbon microtube sponge electrocatalyst for oxygen reduction and oxygen evolution reactions. Energy Environ Sci 9:3079–3084. https://doi.org/10.1039/C6EE02169G

Li S, Ho SH, Hua T, Zhou Q, Tang J (2020) Sustainable biochar as electrocatalysts for the oxygen reduction reaction in microbial fuel cells. Green Energy Environ 6:644–659. https://doi.org/10.1016/j.gee.2020.11.010

Li S, Ho S-H, Hua T, Zhou Q, Li F, Tang J (2021) Sustainable biochar as an electrocatalysts for the oxygen reduction reaction in microbial fuel cells. Green Energy Environ 6:644–659. https://doi.org/10.1016/j.gee.2020.11.010

Li S, Feng C, Xie Y, Guo C, Zhang L, Wang J (2022) Synthesis of nitrogen-rich porous carbon nanotubes coated Co nanomaterials as efficient ORR electrocatalysts via MOFs as precursor. J Alloys Compd 911:165060. https://doi.org/10.1016/j.jallcom.2022.165060

Liang J, Tang D, Huang L, Chen Y, Ren W, Sun J (2018) High oxygen reduction reaction performance nitrogen-doped biochar cathode: a strategy for comprehensive utilizing nitrogen and carbon in water hyacinth. Bioresour Technol 267:524–531. https://doi.org/10.1016/j.biortech.2018.07.085

Liu J, Song P, Ruan M, Xu W (2016) Catalytic properties of graphitic and pyridinic nitrogen doped on carbon black for oxygen reduction reaction. Chin J Catal 37:1119–1126. https://doi.org/10.1016/S1872-2067(16)62456-7

Liu H, Cheng J, Lu Z, Huang X, Zhu Y, Zhao X, Wang T, Masa J, Chen X (2019) Significant enhancement of the oxygen reduction activity of self-heteroatom doped coal derived carbon through oxidative pretreatment. Electrochim Acta 312:22–30. https://doi.org/10.1016/j.electacta.2019.04.171

Liu C, Li Y, Cui J, Qian Z, Liu D (2022a) Fabrication of ORR/OER Electrocatalysts with simple one-step strategy from sustainable cornstalks. Catal Commun 171:106525. https://doi.org/10.1016/j.catcom.2022.106525

Liu M, Xu Q, Miao Q, Yang S, Wu P, Liu G, He J, Yu C, Zeng G (2022b) Atomic Co–N4 and Co nanoparticles confined in COF@ZIF-67 derived core–shell carbon frameworks: bifunctional non-precious metal catalysts toward the ORR and HER. J Mater Chem A 10:228–233. https://doi.org/10.1039/D1TA08325B

Ma L-L, Liu W-J, Hu X, Lam PKS, Zeng JR, Yu H-Q (2020) Ionothermal carbonization of biomass to construct sp2/sp3 carbon interface in N-doped biochar as efficient oxygen reduction electrocatalysts. Chem Eng J 400:125969. https://doi.org/10.1016/j.cej.2020.125969

Ma LL, Hu X, Liu WJ, Li HC, Yu HQ (2021) Constructing N, P-dually doped biochar materials from biomass wastes for high-performance bifunctional oxygen electrocatalysts. Chemosphere 278:130508. https://doi.org/10.1016/j.chemosphere.2021.130508

Maliutina K, Huang J, Su T, Yu J, Fan L (2021) Biomass-derived Ta, N, S co-doped CNTs enriched carbon catalyst for efficient electrochemical oxygen reduction. J Alloys Compd 888:161479. https://doi.org/10.1016/j.jallcom.2021.161479

Meng F, Wang D (2020) Effects of vacuum freeze drying pretreatment on biomass and biochar properties. Renew Energ 155:1–9. https://doi.org/10.1016/j.renene.2020.03.113

Najbjerg H, Afseth NK, Young JF, Bertram HC, Pedersen ME, Grimmer S, Vogt G, Kohler A (2011) Monitoring cellular responses upon fatty acid exposure by Fourier transform infrared spectroscopy and Raman spectroscopy. Analyst 136:1649–1658. https://doi.org/10.1039/C0AN00916D

Panomsuwan G, Eiad-ua A, Kaewtrakulchai N, Seizawa A, Ishizaki T (2022) Cattail leaf-derived nitrogen-doped carbons via hydrothermal ammonia treatment for electrocatalytic oxygen reduction in an alkaline electrolyte. Int J Hydrogen Energy 47:24738–24749. https://doi.org/10.1016/j.ijhydene.2022.05.213

Peng X, Zhang L, Chen Z, Zhong L, Zhao D, Chi X, Zhao X, Li L, Lu X, Leng K (2019) Hierarchically porous carbon plates derived from wood as bifunctional ORR/OER electrodes. Adv Mater 31:1900341. https://doi.org/10.1002/adma.201900341

Qunying L, Hong Su, Jing Y, Chunkit L, Shuiliang C (2014) N-doped mesoporous carbon as a bifunctional material for oxygen reduction reaction and supercapacitors. Chin J Catal 35:1078–1083. https://doi.org/10.1016/S1872-2067(14)60044-9

Sun M, Davenport D, Liu H, Qu J, Elimelech M, Li J (2018) Highly efficient and sustainable non-precious-metal Fe–N–C electrocatalysts for the oxygen reduction reaction. J Mater Chem A 6:2527–2539. https://doi.org/10.1039/C7TA09187G

Wan C, Duan X, Huang Y (2020) Molecular design of single-atom catalysts for oxygen reduction reaction. Adv Energy Mater 10:1903815. https://doi.org/10.1002/aenm.201903815

Wang T, Chen Z-X, Chen Y-G, Yang L-J, Yang X-D, Ye J-Y, Xia H-P, Zhou Z-Y, Sun S-G (2018) Identifying the active site of N-doped graphene for oxygen reduction by selective chemical modification. ACS Energy Lett 3:986–991. https://doi.org/10.1021/acsenergylett.8b00258

Wang P, Ye H, Yin YX, Chen H, Bian YB, Wang ZR, Cao FF, Guo YG (2019) Fungi-enabled synthesis of ultra high-surface-area porous carbon. Adv Mater 31:1805134. https://doi.org/10.1002/adma.201805134

Wang J, Li M, Zhang J, Yan Y, Qiu X, Cai B, Yang G, Tang Y (2020) Atom-ratio-conducted tailoring of pdau bimetallic nanocrystals with distinctive shapes and dimensions for boosting the ORR performance. Chem-Eur J 26:4480–4488. https://doi.org/10.1002/chem.201905284

Wang K, Yang J, Liu W, Yang H, Yi W, Sun Y, Yang G (2022) Self-nitrogen-doped carbon materials derived from microalgae by lipid extraction pretreatment: highly efficient catalyst for the oxygen reduction reaction. Sci Total Environ 821:153155. https://doi.org/10.1016/j.scitotenv.2022.153155

Wang Z, Li J, Li Z, Yang G, Zuo X, Cao Y, Li X, Chen G, Yan B (2023) A coupling strategy for comprehensive utilization of distillers' grains towards energy recovery and carbon sequestration. Energ Convers Manage 275:116494

Wannasen L, Chanlek N, Siriroj S, Maensiri S, Swatsitang E, Pinitsoontorn S (2022) Enhanced electrochemical performance of sugarcane bagasse-derived activated carbon via a high-energy ball milling treatment. Nanomaterials 12(20):3555. https://doi.org/10.3390/nano12203555

Wu Y, Chen Y, Wang H, Wang C, Wang A, Zhao S, Li X, Sun D, Jiang J (2018) Efficient ORR electrocatalytic activity of peanut shell-based graphitic carbon microstructures. J Mater Chem A 6:12018–12028. https://doi.org/10.1039/C8TA02839G

Wu P, Kang X, Wang W, Yang G, He L, Fan Y, Cheng X, Sun Y, Li L (2021) Assessment of coproduction of ethanol and methane from pennisetum purpureum: effects of pretreatment, process performance, and mass balance. ACS Sustain Chem Eng 9:10771–10784. https://doi.org/10.1021/acssuschemeng.1c02010

Xiong J, Zhang S, Ke L, Wu Q, Zhang Q, Cui X, Dai A, Xu C, Cobb K, Liu Y, Ruan R, Wang Y (2023) Research progress on pyrolysis of nitrogen-containing biomass for fuels, materials, and chemicals production. Sci Total Environ 872:162214. https://doi.org/10.1016/j.scitotenv.2023.162214

Xu J, Xue B, Liu C, Xia C, Li M, Xiao R (2021) Efficient utilization of crude bio-oil: the synthesis of nitrogen-doped hierarchically porous carbon as electrocatalysts for the oxygen reduction reaction. Sustain Energ Fuels 5:3884–3894. https://doi.org/10.1039/D1SE00652E

Yaashikaa PR, Keerthana Devi M, Senthil Kumar P, Rangasamy G, Rajendran S, Xiao L (2023) A review on pretreatment methods, photobioreactor design and metabolic engineering approaches of algal biomass for enhanced biohydrogen production. Int J Hydrogen Energy 48:21110–21127. https://doi.org/10.1016/j.ijhydene.2022.10.092

Yang W, Li J, Lan L, Fu Q, Zhang L, Zhu X, Liao Q (2018) Poison tolerance of non-precious catalyst towards oxygen reduction reaction. Int J Hydrogen Energy 43:8474–8479. https://doi.org/10.1016/j.ijhydene.2018.03.135

Yang J, Tang S, Song B, Jiang Y, Zhu W, Zhou W, Yang G (2023a) Optimization of integrated anaerobic digestion and pyrolysis for biogas, biochar and bio-oil production from the perspective of energy flow. Sci Total Environ 872:162154. https://doi.org/10.1016/j.scitotenv.2023.162154

Yang J, Yang H, Wang S, Wang K, Sun Y, Yi W, Yang G (2023b) Importance of pyrolysis programs in enhancing the application of microalgae-derived biochar in microbial fuel cells. Fuel 333:126244. https://doi.org/10.1016/j.fuel.2022.126244

Ye S, Shi W, Liu Y, Li D, Yin H, Chi H, Luo Y, Ta N, Fan F, Wang X, Li C (2021) Unassisted photoelectrochemical cell with multimediator modulation for solar water splitting exceeding 4% solar-to-hydrogen efficiency. J Am Chem Soc 143:12499–12508. https://doi.org/10.1021/jacs.1c00802

Zhang L, Xia Z (2011) Mechanisms of oxygen reduction reaction on nitrogen-doped graphene for fuel cells. J Phys Chem C 115:11170–11176. https://doi.org/10.1021/jp201991j

Zhang F, Miao J, Liu W, Xu D, Li X (2019) Heteroatom embedded graphene-like structure anchored on porous biochar as efficient metal-free catalyst for ORR. Int J Hydrogen Energy 44:30986–30998. https://doi.org/10.1016/j.ijhydene.2019.09.239

Zhang JJ, Sun Y, Guo LK, Sun XN, Huang NB (2021) Ball-milling effect on biomass-derived nanocarbon catalysts for the oxygen reduction reaction. ChemistrySelect 6:6019–6028. https://doi.org/10.1002/slct.202100752

Zhou Y, Gu X, Wu J, Huang H, Shao M, Liu Y, Kang Z (2023) Efficient synthesis of H2O2 via oxygen reduction over PANI driven by kinetics regulation of carbon dots. Appl Catal B-Environ 322:122105. https://doi.org/10.1016/j.apcatb.2022.122105